Achieving industrial ammonia synthesis rates at near-ambient conditions through modified scaling relations on a confined dual site

Tao Wang[a,1] and Frank Abild-Pedersen[b,1]

[a]Center of Artificial Photosynthesis for Solar Fuels, School of Science, Westlake University, Hangzhou 310024, China; and [b]SUNCAT Center for Interface Science and Catalysis, Stanford Linear Accelerator Center, Menlo Park, CA 94025

Edited by Alexis T. Bell, University of California, Berkeley, CA, and approved June 17, 2021 (received for review April 6, 2021)

The production of ammonia through the Haber–Bosch process is regarded as one of the most important inventions of the 20th century. Despite significant efforts in optimizing the process, it still consumes 1 to 2% of the worldwide annual energy for the high working temperatures and pressures. The design of a catalyst with a high activity at milder conditions represents another challenge for this reaction. Herein, we combine density functional theory and microkinetic modeling to illustrate a strategy to facilitate low-temperature and -pressure ammonia synthesis through modified energy-scaling relationships using a confined dual site. Our results suggest that an ammonia synthesis rate two to three orders of magnitude higher than the commercial Ru catalyst can be achieved under the same reaction conditions with the introduction of confinement. Such strategies will open pathways for the development of catalysts for the Haber–Bosch process that can operate at milder conditions and present more economically viable alternatives to current industrial solutions.

Haber–Bosch process | milder conditions | confinement | scaling relation | microkinetic modeling

The Haber–Bosch process (1, 2), responsible for converting nitrogen (N_2) and hydrogen (H_2) to ammonia (NH_3), is considered one of the most important inventions of the 20th century (3). The ammonia produced mainly goes to the manufacturing of nitrogenous fertilizer for agriculture (4), but on the downside it consumes 1 to 2% of annual energy usage worldwide related to the high working temperatures (573 to 873 K) and pressures (100 to 350 bar) as well as the use of natural gas–derived H_2 as feedstock (5). Alternatively, some ambient-condition N_2 fixation strategies such as photo- and electrocatalytic methods that rely exclusively on renewable electricity and feedstocks (i.e., hydrogen from water photo/electrolysis) have been widely proposed and investigated. Such alternatives represent more sustainable and promising solutions to reducing energy consumption (6, 7). However, the large-scale application of (photo)electrochemical ammonia synthesis is still facing considerable scientific and technical challenges such as limited NH_3 selectivity, low current density, and poor energy efficiency (8–10). Noteworthy, the century-old Haber–Bosch process is still the predominant source of the world's ammonia production today, representing more than 90% of the annual production (11). Hence, there is an economic incentive to optimize the conventional Haber–Bosch process to operate under milder conditions and to design novel catalysts that are active at lower temperatures and pressures than those known today, which is considered a core scientific challenge in heterogeneous catalysis.

Theoretical investigations have demonstrated that the ammonia synthesis activity of metal-based catalysts is limited by a balance between N_2 dissociation and further hydrogenation of the atomic nitrogen adsorbed on the surface (12, 13). In addition, as shown in Fig. 1*A*, the N_2 dissociation barrier (E_{N-N}) is directly linked to the energy of the final state of the elementary step, i.e., the adsorption energy of atomic N (E_N) through a linear scaling relation (14, 15). Catalysts such as Mo and Re with strong binding of atomic N will have low barriers for N_2 dissociation but will at the same time be poisoned by nitrogen species due to the sluggish kinetics of NH_x hydrogenation, whereas catalysts like Cu and Ag with weak binding of atomic N have fast hydrogenation kinetics but will be unable to activate N_2 at a sufficient rate because of the high energy barrier. Fig. 1*B* shows that ammonia synthesis reaction rates calculated using a mean-field microkinetic model have a volcano-type relationship as a function of E_N governed by the Sabatier principle (16). Therefore, finding an optimal catalyst on which the Haber–Bosch process at low temperature and pressure is feasible requires weak binding of NH_x ($x = 0$, 1, and 2) intermediates to avoid being limited by the hydrogenation step and at the same time have low energy barriers for N_2 dissociation. This clearly necessitates an approach that can circumvent the aforementioned scaling relations between reaction intermediates (17).

Herein, we propose a theoretical strategy to accelerate the ammonia synthesis activity of metal catalysts by modifying the scaling relations with the help of a special confined dual site, where the typical confinement has been experimentally proven to be able to increase reaction rates, enhance selectivity, and stabilize reactive species (18–22). In this work, we show how confinement can impact catalytic processes and illustrate how this can lead to increased reaction rates for the Haber–Bosch process and production of ammonia at near-ambient conditions.

Results

We envision the active sites being confined within a layered structure or nanotube as shown in Fig. 1*C*. Strictly speaking, this is not the typical confinement strategy as reported in the literature (23), where a second coordination sphere surrounding the active site is

Significance

The Haber–Bosch process is of significance in producing fertilizer for agricultural needs and to avoid worldwide mass starvation. Designing a state-of-the-art catalyst to achieve a mild-condition Haber–Bosch process represents a great challenge because it consumes 1 to 2% of annual energy usage worldwide. We propose a theoretical strategy with a confined dual site to achieve an ammonia synthesis rate two to three orders of magnitude higher than the commercial Ru catalyst under the same reaction conditions. This work will open pathways for developing catalysts for the Haber–Bosch process that can operate under milder conditions.

Author contributions: T.W. and F.A.-P. designed research; T.W. performed research; T.W. and F.A.-P. analyzed data; T.W. and F.A.-P. wrote the paper.

The authors declare no competing interest.

This article is a PNAS Direct Submission.

[1]To whom correspondence may be addressed. Email: twang@westlake.edu.cn or abild@slac.stanford.edu.

This article contains supporting information online at https://www.pnas.org/lookup/suppl/doi:10.1073/pnas.2106527118/-/DCSupplemental.

Published July 19, 2021.

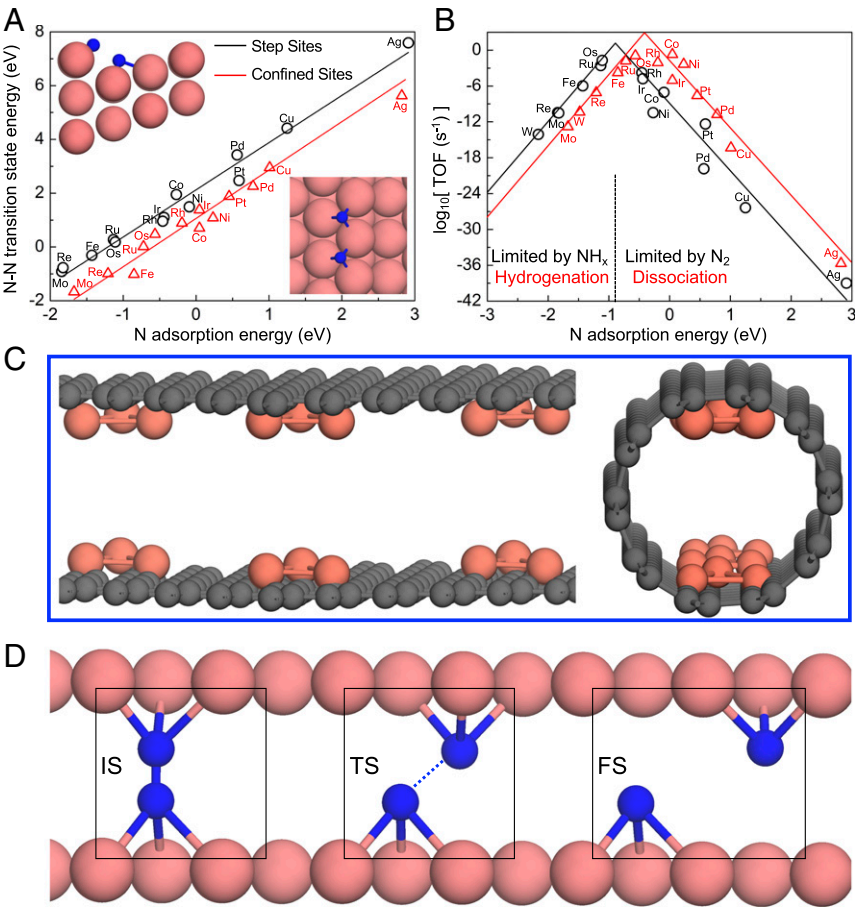

Fig. 1. Key factors and challenges in ammonia synthesis. (*A*) The DFT calculated transition state energies of N_2 dissociation as a function of nitrogen adsorption energies on the step sites of transition metals (black circles) and under confinement (red triangles). (*B*) Corresponding theoretically simulated volcano plots of the ammonia synthesis activity (TOF) as a function of nitrogen adsorption energies at 673 K, p_{N2} = 24.5 bar, p_{H2} = 74.25 bar, p_{NH3} = 1 bar at 2% conversion. (*C*) Schematic illustration of the confined dual sites in a layered graphene structure and inside a carbon nanotube. (*D*) The N_2 dissociation mechanism under confined dual sites (pink, gray, and blue spheres denote metal, carbon, and nitrogen atoms, respectively; IS, TS, and FS denote initial, transition, and final states, respectively).

constructed to affect the gas diffusion and adsorption as well as phase transformations within such a microenvironment (24). Usually, the metal sites are anchored inside the carbon nanotube without another metal site in the vicinity. To model the complex microenvironment of such confined dual sites, we used low-index close-packed metal surfaces to construct an interfacial structure with an optimal interspatial distance for each metal. As illustrated in Fig. 1*D*, N_2 molecules activated by such a dual-site structure will undergo a dissociation mechanism which is promoted by the decoupling in the transition state of the active-site components on the metal catalyst system. The ability of a transition metal to activate N_2 is attributed to the electronic structure of the metal d-states in which empty and occupied d orbitals accept the electrons from N_2 and simultaneously back-donate electrons into N_2 antibonding orbitals to weaken the N≡N triple bond (25). The confined dual sites, as depicted in Fig. 1*D*, provide the optimal stabilization of the N_2 transition state as seen by the calculated results in Fig. 1*A*, where most metal catalysts have lower energy barriers for N_2 activation under such confined conditions. Our microkinetic modeling results in Fig. 1*B* indicate that the confined metallic catalysts can have ammonia synthesis activity up to two to three orders of magnitude higher than the known optimal Ru catalyst under the same reaction conditions, which opens an avenue for designing catalysts for the Haber–Bosch process working at low temperatures and low pressures.

In our study, a large group of transition metals are chosen as model catalysts, i.e., the face-centered cubic (FCC) Cu, Ag, Au, Ni, Pt, Pd, Rh, and Ir; hexagonal close-packed (HCP) Co, Ru, Re, and Os; and body-centered cubic (BCC) Fe, Mo, and W. All simulations are performed with the BEEF-vdW functional (26), which has proven to be able to adequately describe the reaction mechanism and rates of ammonia synthesis on transition metals (27). The close-packed surface, i.e., lowest-energy surface, of each metal is used to construct the confined systems shown schematically in Fig. 1*D*, and different values of distance ranging from 12 Å to 4 Å are considered to identify the optimal distance of each metal with the most stable N_2 adsorption. Each metal has a different optimal distance, i.e., 4.0 Å for Fe, Ni, Ru, Re, and Os; 4.2 Å for Co, W, Mo, and Rh; 4.3 Å for Cu, Pt, Ag, and Au; and 4.5 Å for Pd. A more detailed description of the procedure and the computational details is provided in *SI Appendix*. The full ammonia synthesis reaction mechanism including H_2 and N_2 dissociation, hydrogenation of NH_x (x = 0 to 2) species, and adsorption/desorption of reactants and products is systematically calculated with density functional theory (DFT) on these confined systems. To facilitate a comprehensive and accurate comparison between calculations on the confined systems and systems without confinement, similar systematic calculations were carried out on the close-packed and stepped metal surfaces of all 15 transition metals, representing the most comprehensive dataset for theoretically

simulated ammonia synthesis reaction mechanism on different active sites of versatile metals. The coordinates of all the optimized adsorbates and transition state structures as well as formation energies are included in Dataset S1.

Based on all these calculations, descriptor-based microkinetic models (28, 29) were established to map out the general trends in ammonia synthesis of the different transition metals under different reaction conditions. In Fig. 2 *A*–*C*, the turnover frequencies (TOF) of terrace, step, and confined terrace sites of various transition metals for ammonia production are plotted as a function of nitrogen adsorption energy and N_2 dissociation energy barrier under typical Haber–Bosch process working conditions at 673 K, $p_{N2} = 24.5$ bar, $p_{H2} = 74.25$ bar, and $p_{NH3} = 1$ bar, corresponding to 2% conversion. The inlet gas mixtures were limited to pure N_2 and H_2 without considering other impurities such as O_2 and H_2O in the kinetic modeling. It clearly shows that the ammonia synthesis activity is strongly dependent on the nature of the active site and the metal. For example, the terrace sites in Fig. 2*A* have very limited activity compared to the step sites in Fig. 2*B*, indicating the important role of undercoordinated sites in breaking the strong N_2 bond and hence defining the higher ammonia synthesis activity, which is also in line with previous experimental and theoretical findings (30). In addition, Fe and Ru catalysts are very close to the plateau on the activity volcanos, which explains the unique role these materials play in practical industrial applications for ammonia synthesis today (2). We note that the undercoordinated site on metallic Os is very close to the top of volcano as well. Indeed, Os was identified early on by Fritz Haber to be an active catalyst for ammonia synthesis (1) but was discarded because of its scarcity as well as its high cost. It is clear that our descriptor-based kinetic model applied provides a simple rationale for the general ammonia activity trend of different metals and their surface orientations, which agrees well with available experimental and theoretical knowledge (4, 12, 13, 31–33).

On the confined dual sites, very interesting activity trends for the different metals are observed as shown in Fig. 2*C*. A different volcano appears where adsorption follows the trend on the terrace sites, whereas N_2 dissociation follows a hitherto unknown behavior due to the decoupling of metal atoms defining the active site. However, all metals still follow a similar linear scaling relation between nitrogen adsorption energy and the N–N transition state energy on confined dual sites, where Fe and Co metals show slightly larger deviations from the scaling line. The resulting shift leads to an increased activity for all transition metals as compared to the terrace and step sites. On this volcano, Co is on the high-activity plateau, with an ammonia synthesis rate two to three orders of magnitude higher than a stepped Ru catalyst, which is the most active catalyst known. Close inspections reveal that the confined Co system has a much lower energy barrier for N_2 dissociation than both the terrace and step sites. This, combined with a relatively weak N binding strength, leads to a deviation from the typical scaling relations for the reaction and therefore meets the criteria for being an optimal ammonia synthesis catalyst. Note that the increase in ammonia synthesis activity for the confined catalyst compared with the step sites is a general trend among different metals, as clearly revealed in Fig. 3*A*, i.e., nine orders of magnitude increase for Co, five for Ni, and two for Fe. Two factors can cause increasing rates: 1) higher intrinsic activity or 2) an increase in the number of active sites. Prior studies on Ru have shown that step sites have a nine orders of magnitude higher activity than terrace sites, and even though a typical Ru catalyst only has ~1% step sites they clearly dominate the reactivity (30). Similarly, the confined dual sites studied herein with, in the case of Co, an additional two to three orders of magnitude higher activity than Ru step sites, have the potential to increase the TOF further even if only a small number of active sites are available. Confinement as modeled in this study clearly represents an ideal structure of the active site, and such sites could potentially be achieved using certain practical experimental strategies, like incorporating small metal nanoparticles inside carbon nanotubes with dual sites optimized for the relevant reaction steps. In addition, the two-dimensional (2D) materials MXenes also represent a group of candidates to achieve the above-mentioned goal. For example, the layered MoS_2 could provide an ideal confinement between two layers, where the interspaces can also be adapted with state-of-the-art experimental strategies, which makes it possible to decorate metal atoms/clusters on both sides of MoS_2. We note that incorporating metal clusters inside carbon nanotubes to construct the dual active sites introduces

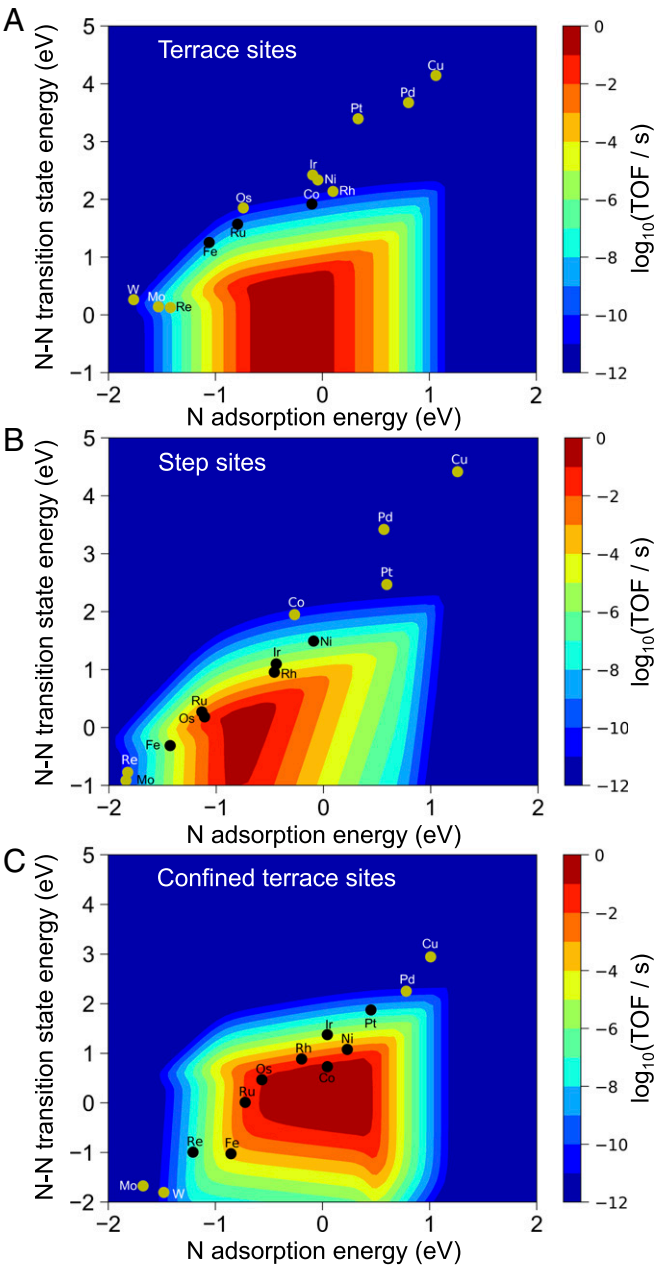

Fig. 2. Ammonia synthesis activity volcano maps on different active sites. Calculated ammonia synthesis rates as a function of the nitrogen adsorption energy and the N–N transition-state energy on (*A*) metal terraces sites, (*B*) step sites, and (*C*) confined terraces sites of transition metals. (Reaction conditions: 673 K, $p_{N2} = 24.5$ bar, $p_{H2} = 74.25$ bar, $p_{NH3} = 1$ bar corresponding to 2% conversion.)

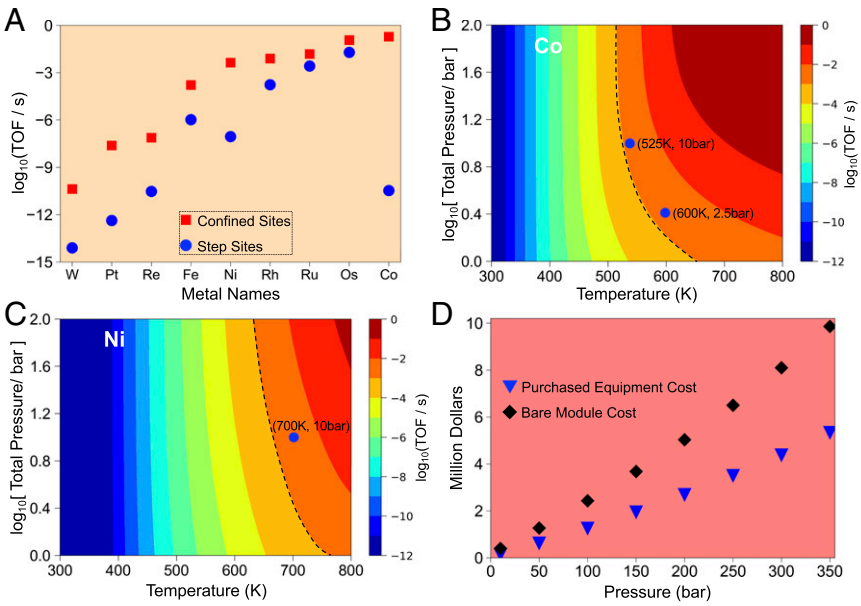

Fig. 3. Improved ammonia synthesis activity with confinement and corresponding economic analysis. (A) Activity difference between confined sites and step (211) sites. Elements are ordered left to right according to their increasing TOF under confinement. (*B* and *C*) Ammonia synthesis rate (TOF) at $N_2/H_2 = 1/3$ as a function of temperature and total pressure on confined Co and Ni catalysts, respectively. (*D*) Effect of working pressure on capital costs of a 63-m^3 vessel made from carbon steel for industrial ammonia synthesis (the black dashed lines in *B* and *C* denote the activity range of a stepped Ru catalyst at 673 K, $p = 100$ bar, N_2/H_2 gas ratio of 1/3, and 2% conversion).

significant challenges both from a synthesis and a stability perspective. The stability and catalytic fluctuation of small metal particles have been studied extensively by Sautet and coworkers (34–36), and they have demonstrated the essential role of fluxionality, restructuring, dynamics, and an ensemble of metastable states in determining the catalytic performances of metal clusters under working conditions. Therefore, further studies of such dual active sites should explicitly account for the stability and fluxionality. With such significant improvements, catalyst engineering with higher ammonia activity at lower temperature and lower pressure using confinement become possible.

To evaluate under what conditions we can run the Haber–Bosch process with comparable rates under confinement as measured on a stepped Ru catalyst we analyze how the ammonia synthesis activity depends on reaction conditions on two of the most active noble-metal-free catalysts in Fig. 2*C*, i.e., Co and Ni. Fig. 3 *B* and *C* show the ammonia synthesis activity on Co and Ni as a function of temperature and total pressure with an N_2/H_2 gas ratio of 1/3. The black dashed lines indicate the calculated activity of the stepped Ru catalyst at 673 K, $p = 100$ bar, $N_2/H_2 = 1/3$, and 2% conversion. In principle, the Co catalyst under confinement shown in Fig. 3*B* can have ammonia synthesis activity comparable to Ru step sites at low temperature and pressure. i.e., at 525 K with a total pressure ~10 bar and at 600 K with a total pressure ~2.5 bar. Similarly, the confined Ni catalyst shown in Fig. 3*C* also has the possibility to perform better than the Ru catalyst when running at 700 K with a total pressure around 10 bar. The pressure reduction carries an important financial incentive, and we have performed an economic analysis to describe the direct reduction of capital cost. Clearly, our economic assessment is based on the hypothesis that the proposed confined dual sites can be synthesized successfully with state-of-the-art experimental techniques. Fig. 3*D* shows the equipment cost and the bare module cost as a function of operating pressure, calculated using the Capcost_2017 program as developed based on the textbook *Analysis, Synthesis and Design of Chemical Processes* (37). As an example, the purchased equipment cost (bare module cost) for a typical 63-m^3 ammonia synthesis vessel made from carbon steel requires a roughly $5.34 (9.86) million investment when operating at a pressure of 350 bar. This number decreases to only $0.15 (0.40) million at operating pressures around 10 bar. This analysis clearly reflects a dramatic decrease in capital cost of ammonia production via the Haber–Bosch process if the catalyst could operate at lower reaction pressures, as is shown to be possible with the confinement strategy introduced in this article.

Conclusion

In summary, we have introduced a theoretical framework outlining how confined dual sites can facilitate the ammonia synthesis reaction under milder conditions through modification of the established scaling relations between the N_2 dissociation barrier and atomic N adsorption energy. Our results show that a catalyst with confined dual sites can have an ammonia synthesis rate two to three orders of magnitude higher than the undercoordinated sites on a Ru catalyst, the most active ammonia synthesis catalyst used industrially, under the same reaction conditions. We find that confined dual terrace sites have much lower N_2 dissociation energy barriers than both terrace and step sites and at the same time maintain a weak N binding strength, thus meeting the criteria for being an optimal ammonia synthesis catalyst. Considering their much higher activities, even if only a small number of such confined dual active sites are available this can still dramatically increase the TOF of the Haber–Bosch process. Despite the fact that confinement as modeled in this study clearly represents an ideal structure of the active site, it works as a potentially promising conceptual strategy for reducing energy consumption in ammonia production. Such sites could potentially be achieved using certain practical experimental strategies, like incorporating small metal nanoparticles inside carbon nanotubes or 2D materials with a double-sided structure optimized for the relevant reaction steps. We anticipate that the confinement strategy proposed in this work will open avenues for the design of low-temperature and lower-pressure Haber–Bosch catalysts at much lower capital and operational cost. Further state-of-the-art experimental efforts are

essential and highly desired to engineer such catalytic systems for practical applications, which represent significant contributions to sustainable energy and advances in heterogeneous catalysis.

Materials and Methods

Computational Details. All computations were carried out using a periodic plane-wave-based DFT method as implemented in Quantum Espresso code (38) with pseudopotentials GBRV version 1.5 (39). The energy cutoffs for plane wave and electron density were set to be 500 eV and 5,000 eV, respectively. The BEEF-vdW functional was used to describe the exchange correlation contribution to the electronic energy (26). The close-packed surfaces [the (111) facet for FCC metal, the (0001) facet of HCP metal, and the (110) facet for BCC metal] were simulated using seven-layer 2×2 supercells with the topmost two layers relaxed and the bottom five layers constrained. The $(4 \times 4 \times 1)$ Monkhorst–Pack k-point grids were applied for sampling. The stepped surfaces [the (211) facet for FCC metal and the (210) facet for BCC metal] were simulated with 12-layer 3×3 supercells with the topmost four layers relaxed and the bottom eight layers constrained. A $(3 \times 3 \times 1)$ Monkhorst–Pack k-point grid was applied for sampling. Structure optimizations were done until forces became smaller than 0.05 eV/Å and the energy difference was lower than 10^{-5} eV. A vacuum layer of 12 Å was set between periodically repeated slabs for the normal surfaces without confinement. Spin polarization was included for Fe, Co, and Ni systems to correctly describe magnetic properties. Transition-state geometries were located with the climbing-image nudged elastic band method (40). The vibration frequencies for all species were calculated to analyze thermodynamic contributions to free energies. The thermodynamic enthalpies and entropies were calculated using the harmonic potential approximation for surface adsorbates and an ideal gas approximation for gas phase species. The calculated gas-phase enthalpy change of the ammonia synthesis $N_2 + 3H_2(g) \rightarrow 2NH_3(g)$ at 298 K with BEEF-vdW functional and an ideal gas approximation is −92.14 kJ/mol, which is in good agreement with the experimental value of −91.8 kJ/mol and indicates the reliability of our theoretical method in correctly describing the gas-phase thermodynamics. The formation energies (ΔE) of all the species are calculated relative to gaseous N_2 and H_2 as $\Delta E_{NxHy} = E(N_xH_y) - E(\text{slab}) - x*E_{N2}/2 - y*E_{H2}/2$, where $E(N_xH_y)$, $E(\text{slab})$, E_{N2}, and E_{H2} denote the electronic energies of the surface slab with adsorbates, clean surface slab, and gas-phase N_2 and H_2 molecules, respectively. The Gibbs free energy (ΔG) at different temperatures is calculated with $\Delta G_{NxHy} = \Delta E_{NxHy} + \Delta ZPE - T\Delta S$, where the enthalpy and entropic contributions are calculated within the harmonic approximation for surface species and the ideal gas approximation for gas-phase species. The CatMAP code (41) was applied to solve the differential equations in our mean-field microkinetics modeling and calculate TOF of ammonia synthesis at descriptor spaces and different reaction conditions.

Data Availability. Optimized coordinates have been deposited at Catalysis-Hub.org (https://www.catalysis-hub.org/publications/WangAchieving2021). The code used to perform the microkinetics modeling this work is available at GitHub (https://github.com/SUNCAT-Center/catmap). All other study data are included in the article and/or supporting information.

ACKNOWLEDGMENTS. T.W. acknowledges start-up funds from Westlake University and the Westlake University HPC Center for computation support. We thank Professor Licheng Sun for insightful discussions and helpful suggestions to this project. The authors acknowledge support from the US Department of Energy (DOE), Office of Science, Office of Basic Energy Sciences, Chemical Sciences, Geosciences, and Biosciences Division, Catalysis Science Program to the SUNCAT Center for Interface Science and Catalysis and the use of computer time at the National Energy Research Scientific Computing Center, a DOE Office of Science User Facility supported by the Office of Science of the US DOE under Contract DE-AC02-05CH11231.

1. F. Haber, G. van Oordt, Über die Bildung von Ammoniak den Elementen. *Z. Anorg. Chem.* **44**, 341–378 (1905).
2. J. R. Jennings, *Catalytic Ammonia Synthesis: Fundamentals and Practice* (Plenum Press, New York, 1991).
3. V. Smil, Detonator of the population explosion. *Nature* **400**, 415 (1999).
4. G. Ertl, Reactions at surfaces: From atoms to complexity (Nobel Lecture). *Angew. Chem. Int. Ed. Engl.* **47**, 3524–3535 (2008).
5. J. G. Chen *et al*., Beyond fossil fuel-driven nitrogen transformations. *Science* **360**, 873 (2018).
6. J. K. Nørskov, J. G. Chen, "Sustainable ammonia synthesis—Exploring the scientific challenges associated with discovering alternative, sustainable processes for ammonia production" (US Department of Energy, 2016).
7. L. Ye, R. Nayak-Luke, R. Bañares-Alcántara, E. Tsang, Reaction: "Green" ammonia production. *Chem* **3**, 712–714 (2017).
8. S. Z. Andersen *et al*., A rigorous electrochemical ammonia synthesis protocol with quantitative isotope measurements. *Nature* **570**, 504–508 (2019).
9. B. H. R. Suryanto *et al*., Challenges and prospects in the catalysis of electroreduction of nitrogen to ammonia. *Nat. Catal.* **2**, 290–296 (2019).
10. D. R. MacFarlane *et al*., A roadmap to the ammonia economy. *Joule* **4**, 1186–1205 (2020).
11. L. Wang *et al*., Greening ammonia toward the solar ammonia refinery. *Joule* **2**, 1055–1074 (2018).
12. K. Honkala *et al*., Ammonia synthesis from first-principles calculations. *Science* **307**, 555–558 (2005).
13. A. J. Medford *et al*., From the Sabatier principle to a predictive theory of transition-metal heterogeneous catalysis. *J. Catal.* **328**, 36–42 (2015).
14. F. Abild-Pedersen *et al*., Scaling properties of adsorption energies for hydrogen-containing molecules on transition-metal surfaces. *Phys. Rev. Lett.* **99**, 016105 (2007).
15. R. A. van Santen, M. Neurock, S. G. Shetty, Reactivity theory of transition-metal surfaces: A Brønsted-Evans-Polanyi linear activation energy-free-energy analysis. *Chem. Rev.* **110**, 2005–2048 (2010).
16. M. Che, Nobel Prize in chemistry 1912 to Sabatier: Organic chemistry or catalysis? *Catal. Today* **218–219**, 162–171 (2013).
17. J. Perez-Ramírez, N. Lopez, Strategies to break linear scaling relationships. *Nat. Catal.* **2**, 971–976 (2019).
18. X. Guo *et al*., Direct, nonoxidative conversion of methane to ethylene, aromatics, and hydrogen. *Science* **344**, 616–619 (2014).
19. J. Xiao, X. Pan, S. Guo, P. Ren, X. Bao, Toward fundamentals of confined catalysis in carbon nanotubes. *J. Am. Chem. Soc.* **137**, 477–482 (2015).
20. A. B. Grommet, M. Feller, R. Klajn, Chemical reactivity under nanoconfinement. *Nat. Nanotechnol.* **15**, 256–271 (2020).
21. M. G. Wang *et al*., Mechanism of the accelerated water formation reaction under interfacial confinement. *ACS Catal.* **10**, 6119–6128 (2020).
22. L. Tang, X. Meng, D. Deng, X. Bao, Confinement catalysis with 2D materials for energy conversion. *Adv. Mater.* **31**, e1901996 (2019).
23. S. Guo *et al*., Probing the electronic effect of carbon nanotubes in catalysis: NH(3) synthesis with Ru nanoparticles. *Chemistry* **16**, 5379–5384 (2010).
24. V. Mouarrawis, R. Plessius, J. I. van der Vlugt, J. N. H. Reek, Confinement effects in catalysis using well-defined materials and cages. *Front Chem.* **6**, 623 (2018).
25. M. A. Légaré *et al*., Nitrogen fixation and reduction at boron. *Science* **359**, 896–900 (2018).
26. J. Wellendorff *et al*., Density functionals for surface science: Exchange-correlation model development with Bayesian error estimation. *Phys. Rev. B Condens. Matter Mater. Phys.* **85**, 235149 (2012).
27. A. J. Medford *et al*., Catalysis. Assessing the reliability of calculated catalytic ammonia synthesis rates. *Science* **345**, 197–200 (2014).
28. T. Wang *et al*., Rational design of selective metal catalysts for alcohol amination with ammonia. *Nat. Catal.* **2**, 773–779 (2019).
29. T. Wang, G. Li, X. Cui, F. Abild-Pedersen, Identification of earth-abundant materials for selective dehydrogenation of light alkanes to olefins. *Proc. Natl. Acad. Sci. U.S.A.* **118**, e2024666118 (2021).
30. S. Dahl *et al*., Role of steps in N2 activation on Ru(0001). *Phys. Rev. Lett.* **83**, 1814–1817 (1999).
31. F. Haber, "Nobel Prize Lecture 1918" in *Nobel Lectures: Chemistry 1901–1921* (Elsevier, Amsterdam, 1966).
32. C. Bosch, "Nobel Prize Lecture 1931" in *Nobel Lectures: Chemistry 1922–1941* (Elsevier, Amsterdam, 1966).
33. A. Vojvodic *et al*., Exploring the limits: A low-pressure, low-temperature Haber–Bosch process. *Chem. Phys. Lett.* **588**, 108–112 (2014).
34. G. Sun, P. Sautet, Metastable structures in cluster catalysis from first-principles: Structural ensemble in reaction conditions and metastability triggered reactivity. *J. Am. Chem. Soc.* **140**, 2812–2820 (2018).
35. G. Sun, A. N. Alexandrova, P. Sautet, Pt_8 cluster on alumina under a pressure of hydrogen: Support-dependent reconstruction from first-principles global optimization. *J. Chem. Phys.* **151**, 194703 (2019).
36. H. Guo, P. Sautet, A. N. Alexandrova, Reagent-triggered isomerization of fluxional cluster catalyst via dynamic coupling. *J. Phys. Chem. Lett.* **11**, 3089–3094 (2020).
37. R. Turton, R. C. Bailie, W. B. Whiting, J. A. Shaeiwitz, *Analysis, Synthesis and Design of Chemical Processes* (Pearson Education, ed. 5, 2018).
38. P. Giannozzi *et al*., QUANTUM ESPRESSO: A modular and open-source software project for quantum simulations of materials. *J. Phys. Condens. Matter* **21**, 395502 (2009).
39. K. F. Garrity, J. W. Bennett, K. M. Rabe, D. Vanderbilt, Pseudopotentials for high-throughput DFT calculations. *Comput. Mater. Sci.* **81**, 446–452 (2014).
40. G. Henkelman, B. P. Uberuaga, H. Jonsson, A climbing image nudged elastic band method for finding saddle points and minimum energy paths. *J. Chem. Phys.* **113**, 9901–9904 (2000).
41. A. J. Medford *et al*., CatMAP: A software package for descriptor-based microkinetic mapping of catalytic trsends. *Catal. Lett.* **145**, 794–807 (2015).